HHS Public Access

Author manuscript

Nat Neurosci. Author manuscript; available in PMC 2019 July 02.

Published in final edited form as:

Nat Neurosci. 2019 May ; 22(5): 719–728. doi:10.1038/s41593-019-0372-9.

Senolytic therapy alleviates Aβ-associated oligodendrocyte progenitor cell senescence and cognitive deficits in an Alzheimer's disease model

Peisu Zhang[1,*], **Yuki Kishimoto**[1], **Ioannis Grammatikakis**[2], **Kamalvishnu Gottimukkala**[3], **Roy G. Cutler**[1], **Shiliang Zhang**[4], **Kotb Abdelmohsen**[2], **Vilhelm A. Bohr**[5], **Jyoti Misra Sen**[3,6], **Myriam Gorospe**[2], and **Mark P. Mattson**[1,7,*]

[1]Laboratory of Neurosciences, National Institute on Aging Intramural Research Program, NIH, Baltimore, MD, USA.

[2]Laboratory of Genetics and Genomics, National Institute on Aging Intramural Research Program, NIH, Baltimore, MD, USA.

[3]Laboratory of Clinical Investigation, National Institute on Aging Intramural Research Program, NIH, Baltimore, MD, USA.

[4]Electron Microscopy Core, National Institute on Drug Abuse Intramural Research Program, NIH, Baltimore, MD, USA.

[5]Laboratory of Molecular Gerontology, National Institute on Aging Intramural Research Program, NIH, Baltimore, MD, USA.

[6]Immunology Program, Department of Medicine, Johns Hopkins University School of Medicine, Baltimore, MD, USA.

[7]Department of Neuroscience, Johns Hopkins University School of Medicine, Baltimore, MD, USA.

Abstract

Neuritic plaques, a pathological hallmark in Alzheimer's disease (AD) brains, comprise extracellular aggregates of amyloid-beta (Aβ) peptide and degenerating neurites that accumulate autolysosomes. We found that, in the brains of patients with AD and in AD mouse models, Aβ plaque-associated Olig2- and NG2-expressing oligodendrocyte progenitor cells (OPCs), but not

[*]**Correspondence and requests for materials** should be addressed to P.Z. or M.P.M. zhangpei@mail.nih.gov; mark.mattson@nih.gov.

Author contributions

P.Z. designed and performed the experiments, analyzed the data, and wrote the manuscript. Y.K. performed the experiments and analyzed the data. I.G., K.A., S.Z., R.G.C., and J.T. generated the data. K.G. and J.M.S. generated and characterized the p16-ZsGreen reporter and the APP/PS1 and p16-ZsGreen reporter mice. M.P.M., M.G., and V.A.B. contributed to the experimental design and writing of the manuscript.

Competing interests

The authors declare no competing interests.

Supplementary information is available for this paper at https://doi.org/10.1038/s41593-019-0372-9.

Data availability

The data used to generate the figures in this study are available from the corresponding authors upon reasonable request.

astrocytes, microglia, or oligodendrocytes, exhibit a senescence-like phenotype characterized by the upregulation of p21/CDKN1A, p16/INK4/CDKN2A proteins, and senescence-associated β-galactosidase activity. Molecular interrogation of the Aβ plaque environment revealed elevated levels of transcripts encoding proteins involved in OPC function, replicative senescence, and inflammation. Direct exposure of cultured OPCs to aggregating Aβ triggered cell senescence. Senolytic treatment of AD mice selectively removed senescent cells from the plaque environment, reduced neuroinflammation, lessened Aβ load, and ameliorated cognitive deficits. Our findings suggest a role for Aβ-induced OPC cell senescence in neuroinflammation and cognitive deficits in AD, and a potential therapeutic benefit of senolytic treatments.

AD is an age-related neurodegenerative brain disorder for which there are no disease-modifying treatments. Local inflammation, the presence of activated microglia and astrocytes, lysosome dysfunction, and neuritic degeneration occur in the Aβ plaque environment in vulnerable brain regions in AD[1–4]. Tissues affected in many age-related diseases exhibit accumulations of senescent cells with distinct phenotypes characterized by cell cycle arrest, resistance to apoptosis, and the secretion of proinflammatory molecules[5,6]. Recent findings suggest replicative senescence as a common feature of, and contributor to, aging and the pathogenesis of age-related diseases such as cancer and atherosclerosis[7–9]. Accordingly, the elimination of senescent cells via genetic[7,8] and/or pharmacological[9,10] approaches can extend the health span in aging mice. However, it is not known whether cellular senescence is involved in the pathogenesis of Aβ plaques and associated cognitive impairment in AD.

It was recently reported that astrocytes and microglia accumulate in the Aβ plaque environment[3,4] and exhibit senescence phenotypes in the brains of transgenic mouse models of frontotemporal dementia, a disorder characterized by extensive neuronal tau pathology but no Aβ plaque pathology[11,12]. The third major type of glial cell is the oligodendrocytes, which arise from oligodendrocyte progenitor cells (OPCs). OPCs are a major population of cells in the brain, which are mobilized in response to neuronal injury and demyelination[13–16]. Despite their widespread presence throughout the brain, and their abilities to proliferate and move to and accumulate at sites of neuronal degeneration, the roles for OPCs in AD are unknown. In the present study, we document the presence of OPCs exhibiting a senescence phenotype in the Aβ plaque environment of brains of patients with AD and a transgenic mouse model of AD. Direct exposure to Aβ causes senescence of OPCs, which then become sensitive to being killed by a senolytic cocktail of dasatinib plus quercetin (D + Q). Finally, we show that D + Q senolytic treatment removes senescent OPCs and ameliorates Aβ plaque-associated inflammation and cognitive deficits in AD mice, suggesting a potential for senolytic therapy in AD.

Results

To determine whether OPCs are associated with Aβ plaques, we used antibodies recognizing Aβ, Olig2 (OPC marker) and CDKN1A (p21; a senescence marker and transcriptional target of p53), to perform triple-label immunostaining of brain tissue sections from the inferior parietal cortex of eight patients with AD, eight patients with mild cognitive impairment

(MCI), and eight age-matched, neurologically normal, non-demented control (NDC) subjects (see Supplementary Table 1 for subject age, gender, and Braak/neurofibrillary tangle staging). To reduce autofluorescence and enhance signal-to-noise ratios in fixed human tissue, deparaffinized sections were pretreated with boiling citrate buffer and 75% formic acid before immunostaining (see Supplementary Fig. 1). As expected, Aβ plaques were most abundant in patients with AD, less abundant in patients with MCI, and relatively sparse in NDC groups (Fig. 1a,b). More than 80% of larger Aβ plaques in AD cases (size > 50 μm) contained cells that were immunoreactive with both Olig2 and p21 antibodies; very few or no cells expressed p21 but not Olig2 (Fig. 1a). In contrast, significantly fewer plaques in MCI and NDC subjects exhibited cells co-expressing Olig2 and p21 (Fig. 1a,b). The senescence phenotype of the OPCs was also confirmed using antibodies against a different OPC marker (NG2) and the p53-independent senescence marker p16/INK4/CDKN2A (p16) (Fig. 1c). Senescence marker-positive OPCs were observed in both central and peripheral regions of plaques (Fig. 1a,c). In contrast to OPCs, AD plaque-associated astrocytes (glial fibrillary acidic protein (GFAP)-immunoreactive cells) and microglia (Iba1-immunoreactive cells) did not exhibit a senescence phenotype (see Supplementary Fig. 2).

A common marker of cellular senescence[17], senescence-associated β-galactosidase (SA-βGal) activity, becomes detectable as a result of elevated expression of lysosomal β-D-galactosidase in response to lysosomal stress[18,19]. However, SA-βGal is undetectable in formalin-fixed and paraffin-embedded human tissues. To circumvent this problem, we employed transgenic mice expressing mutant forms of human amyloid precursor protein (APP) and presenilin-1 (PS1), which cause early onset, familial AD (APP/ PS1 mutant mice)[20]. We stained free-floating brain sections from 7.5-month-old APP/PS1 mutant mice for SA-βGal activity, followed by post-fixation in paraformaldehyde and Aβ immunohistochemistry. As expected, Aβ plaques were abundant in the hippocampus and cerebral cortex of APP/PS1 mutant mice and were absent in age-matched wild-type controls (Fig. 2a,b). SA-βGal$^+$ cells were associated with large (>40 μm) Aβ plaques in the entorhinal cortex and hippocampus of APP/PS1 mice (Fig. 2b). Aβ plaques and plaque-associated SA-βGal staining was negligible in 3-month-old APP/PS1 mice, but increased significantly by age 7.5 months (Fig. 2c,d; see Supplementary Fig. 3). Except for neurons, which have previously been reported to exhibit diffuse SA-βGal positivity unrelated to other replicative senescent phenotypes[21], SA-βGal staining was not observed in the hippocampus of wild-type mice (Fig. 2a).

As Aβ deposits accumulate extracellularly, we examined the spatial relationship between senescent cells and Aβ plaques. We employed a high-resolution three-dimensional confocal in situ hybridization (RNAscope-ISH) method to determine whether cells expressing *p16* mRNA were present within and/or surrounding Aβ plaques. We first validated the method by hybridizing negative and positive control probes in 10-μm frozen brain sections from 8-month-old APP/PS1 mice (see Supplementary Fig. 4a,b). We then examined a probe that specifically recognized the mRNA encoding p16 in hippocampal sections of wild-type and APP/PS1 mice. We observed that, in APP/PS1 brain sections, *p16* mRNA puncta were clustered in Aβ-associated cells (Fig. 2e; see Supplementary Videos 1–3). As controls, *p16* mRNA was rare or absent in regions lacking Aβ plaques in APP/PS1 mutant mice, and in wild-type mice (Fig. 2e and see Supplementary Fig. 4c,d). In Supplementary Video 1 *p16*

mRNA is shown in green, Aβ immunoreactivity in red, and cell nuclei in blue (DAPI). In Supplementary Videos 2 and 3 *p16* mRNA is shown in green and LAMP1 protein immunoreactivity in pink or cyan.

Next, we examined the cell type identity of senescent cells. We generated a novel senescence reporter mouse that expresses a bright-green fluorescent protein (ZsGreen) under the control of mouse p16 promoter (see Supplementary Fig. 5a–c and see Methods), and then crossed this mouse line with APP/PS1 double-mutant transgenic mice (see Supplementary Fig. 5d), hereafter referred to as ZsGreen/APPPS1 mice. We found that, in ZsGreen/APPPS1 mouse brains, the localization of ZsGreen cells in Aβ plaques was age dependent, similar to our results in brain sections of APP/PS1 mice double labeled with SA-βGal activity and Aβ immunostaining (Fig. 2d and see Supplementary Fig. 3). At 2.5 months of age, Aβ immunoreactivity was scarcely visible as diffuse deposits, and cells expressing ZsGreen were rare and not associated with Aβ (see Supplementary Fig. 5e). At 4.5 months of age, large Aβ plaques (size>30μm) harbored ZsGreen cells that co-localized with the OPC marker Olig2 and SA-βGal in the cerebral cortex (see Supplementary Fig. 5f). Using an additional panel of glial cell-type-specific antibodies, including CNP for myelinating oligodendrocytes, GFAP for astrocytes, and Iba1 for microglia, we quantitatively validated the glial cell identity of ZsGreen$^+$ senescent cells in Aβ plaques. As shown in Supplementary Fig. 6 and Table 1, 100% of Aβ-associated ZsGreen$^+$cells were Olig2$^+$OPCs, whereas neither GFAP-expressing astrocytes nor Iba1-expressing microglia were ZsGreen$^+$. In addition, ~93% of Aβ-associated oligodendrocytes were ZsGreen-negative.

Because OPCs exhibit a senescent phenotype in the Aβ plaque environment in patients with AD (see Fig. 1), we next determined whether OPC lineage markers were associated with senescence markers in the brains of APP/PS1 transgenic mice. As a control, p21 immunoreactive cells were not observed in the hippocampus of wild-type mice (data not shown). In APP/PS1 mouse brains, NG2- and Olig2-OPC markers co-localized with p21 and p16 immunoactivities in cells associated with Aβ plaques (Fig. 2f; see Supplementary Figs. 7a and 8). On the other hand, GFAP$^+$ astrocytes and Iba1$^+$microglia associated with plaques were not immunoreactive with p16 antibody (see Supplementary Fig. 7b,c), consistent with the results from our analysis of ZsGreen/APP/PS1 mouse brains (see Supplementary Fig. 6a,b) and human AD brains (see Supplementary Fig. 2). As damage to myelinating oligodendrocytes can be a stimulus for the recruitment of OPCs to lesion sites[14–16], we examined the presence of myelin in Aβ plaques of APP/PS1 mouse brains using an anti-myelin basic protein (MBP) antibody. Whereas MBP immunoreactivity associated with presumptive axons was abundant in areas devoid of plaques, the Aβ plaques themselves exhibited little or no MBP immunoreactivity (see Supplementary Fig. 9). Taken together, the data suggest that Aβ-associated OPCs undergo replicative senescence, a previously uncharacterized pathway that would be expected to compromise remyelination in the Aβ plaque environment.

To interrogate the molecular features of plaque-associated cells, we used laser capture microdissection (LCM) to isolate plaque areas and extract RNA to identify expressed mRNAs by quantitative PCR with reverse transcription (RT-qPCR) analysis (see Supplementary Fig. 10). As Aβ plaques are concentrated in the forebrain but not the

cerebellum of APP/PS1 mice[20], we compared forebrain plaque LCM samples with similarly sized, plaque-free tissue from APP/PS1 mouse cerebellum and wild-type mouse forebrain as negative controls. The *hAPP1* mRNA served as a transgene positive control. Compared with plaque-free forebrain tissue from wild-type mice and cerebellar tissue from APP/PS1 mutant mice, LCM plaques were significantly enriched in mRNAs encoding proteins involved in AD pathogenesis[2,3] (*hAPP1*, *Mapt*, *Psen1*, *Notch1*, and *Bace2* mRNAs), OPC lineage (*Cspg4* mRNA, which encodes NG2, *Olig1*, and *Olig2* mRNAs)[13–16,22], cellular senescence (*Cdkn2a* mRNA, which encodes p16), and inflammation (*Il1b* and *Tnfa* mRNAs, which encode interleukin-1β and tumor necrosis factor-α, respectively)[2] (Fig. 3a). Several transcripts upregulated in the plaque environment encode proteins that would be expected to enhance amyloidogenesis (*App* and *Psen1* mRNAs) and/or induce OPC senescence (*Tgfa*, *IL1b*, and *Cdkn2a* mRNAs).

The findings described above indicate that aggregating Aβ may trigger OPC senescence. To test this possibility, we generated OPCs from cultured mouse embryonic stem cells (mESCs) expressing GFP-Olig2 (see Supplementary Fig. 11) and exposed them to aggregating $A\beta_{1–42}$. Whereas no OPCs exhibited SA-βGal activity in control cultures, approximately 10% of the cells exhibited strong SA-βGal activity in cultures exposed to $A\beta_{1–42}$. It was interesting that multiple enlarged SA-βGal$^+$ cells were often located adjacent to each other (Fig. 3b). These findings further support a notion that aggregating $A\beta_{1–42}$ directly triggers OPC senescence, independently of the presence of any other plaque-associated cell types.

To elucidate the ultrastructural features of senescent OPCs and their spatial relationship to Aβ deposits, we employed a double preembedding immunoelectron microscopy technique (see Methods). We examined seven plaque-laden areas (0.5–1 mm^2) in the cerebral cortex of two APP/PS1 mice. In regions where no Aβ deposits were present, Olig2 immunoreactivity (as detected by silver-enhanced gold particles) was localized only in the nucleus of OPCs (Fig. 3c). No Olig2 immunoreactivity was observed in presumptive astrocytes (based on their nuclear morphology), supporting the specificity of the Olig2 immunogold labeling method. In contrast to the areas devoid of Aβ aggregates, plaque-associated OPCs exhibited Olig2 immunoreactivity in the cytoplasm, and these cells were often intimately associated with closely apposed Aβ deposits (Fig. 3d and see Supplementary Figs. 12 and 13). All 24 of 24 Aβ plaque-associated OPCs exhibited cytosolic Olig2, whereas, in all 7 OPCs examined, which were not associated with plaques, the Olig2-associated gold particles were located exclusively in the nucleus. As Olig2 is a transcription factor that plays an important role in the differentiation of OPCs into oligodendrocytes[23,24], the displacement of Olig2 from the nucleus may be linked to the acquisition of a senescence phenotype of OPCs in the Aβ plaque microenvironment. Consistent with the accumulation of LAMP1$^+$autolysosomes[25–27] in senescent cells associated with Aβ plaques (Fig. 2e and see Supplementary Fig. 8c,d), and with evidence that Aβ can directly induce OPC senescence (Fig. 3b), our ultrastructural analysis revealed a dramatic accumulation of autolysosomes in Olig2 immunogold-labeled cells associated with Aβ plaques (Fig. 3d and see Supplementary Figs. 12 and 13). We also observed dystrophic neurites with accumulations of cargo-laden autolysosomes[28] directly adjacent to Olig2-labeled OPCs (Fig. 3e).

A cocktail of two US Federal Drug Administration (FDA)- approved 'senolytic' compounds, dasatinib and quercetin (D + Q), can selectively eliminate senescent cells from pathological tissues[10,29,30], and may thereby counteract age-related pathogenic processes[7–10]. Dasatinib was originally developed as an anti-cancer drug, whereas quercetin is a flavonoid found in many fruits and vegetables. To confirm that D + Q selectively kills senescent cells, we first employed fluorescence-activated cell sorting (FACS) using dodecanoylaminofluorescein di-β-D-galactopyranoside (C_{12}FDG), a fluorogenic β-galactosidase substrate for detecting SA-βGal activity (see Supplementary Fig. 14)[19], along with propidium iodidebased quantification of cell death. To induce classic senescence, Neuro2a (N2a) cells were first exposed to 10 Gy of ionizing radiation, and 5 days later were treated with D + Q for 24 h before FACS analysis. We observed that the decline of senescent cells caused by D + Q was negatively correlated with an increase in cell death in a manner dependent on the dose of D + Q (Fig. 4a). We also found that levels of cleaved caspase-3 increased in response to D + Q treatments, suggesting apoptotic cell death (Fig. 4a; see Supplementary Fig. 14). Furthermore, we observed that, whereas OPCs underwent senescence in response to D + Q exposure, non-senescent OPCs were not killed by D + Q (see Supplementary Fig. 15b,c).

We next determined whether oral administration of D + Q would kill Aβ plaque-associated senescent OPCs in APP/PS1 AD mice. First, we tested the blood-brain barrier permeability of dasatinib and quercetin in 5-month-old APP/PS1 mice receiving dasatinib (12 mg kg^{-1}) and quercetin (50 mg kg^{-1}) by oral gavage. Mass spectrometry analysis revealed that both compounds were readily detectable in the hippocampus and cerebellum of APP/PS1 mice 2 h after D + Q administration (see Supplementary Fig. 16; data not shown). Next, we designed an experiment in which we administered D + Q once daily for 9 days and then quantified Aβ load and Aβ-plaque-associated OPCs, astrocytes, and microglia (Fig. 4b; see Supplementary Fig. 17). We found that this short-term D + Q treatment had no significant effect on Aβ load. Instead, it significantly reduced SA-βGal activity associated with Aβ, as well as the levels of Olig2 and p21 (Fig. 4c). RNAscope-ISH analysis revealed a highly significant decrease in the levels of Aβ-plaque-associated *p16* mRNA in AD mice treated with D + Q compared with those treated with vehicle (Fig. 4d). We also found that acute D + Q administration triggered apoptosis (with a rise in cleaved caspase-3) of SA-βGal-reactive cells associated with Aβ plaque in APP/PS1 mouse brains, but not in the hippocampus of wild-type mice (see Supplementary Fig. 18). Taken together, these in vivo results demonstrate a target-specific effect of acute D + Q treatment on senescent OPCs similar to a recent study using a model of adipose cell senescence[10].

Next, we took advantage of the ZsGreen/APPPS1 p16 reporter mouse AD model (Fig. 4e), and treated these mice for 9 days with D + Q or vehicle and then performed triple-label confocal imaging to establish whether D + Q treatment removed senescent cells, and whether elimination of senescent cells affected plaque-associated inflammation, microglia activation, and/or astrocyte activation. As it was difficult to discern precisely how many senescent cells were involved in forming the senescent cell foci in Aβ plaques (see Supplementary Fig. 6a) due to the high concentration of closely packed cells (see Fig. 2e), we quantified the amount of ZsGreen (p16 reporter) fluorescence/plaque. Treatment with D + Q significantly reduced the amount of Aβ plaque-associated ZsGreen expression (Fig. 4f–h). Senolytic treatment had no significant effect on the numbers of microglia or astrocytes

associated with Aβ plaques (Fig. 4f–h and see Supplementary Figs. 19 and 20). However, microglia in the vehicle group exhibited a condensed morphology with relatively large cell bodies characteristic of an activated inflammatory phenotype (Fig. 4f and see Supplementary Fig. 20), whereas microglia in D + Q-treated groups exhibited deactivated morphologies with ramified processes (Fig. 4g and see Supplementary Fig. 20). This microglial deactivation occurred coincident with the reduction of plaque-associated ZsGreen protein and interleukin-6 protein levels in response to acute D + Q exposure (Fig. 4h and see Supplementary Fig. 21). Interleukin-6 production is a key feature of the senescence-associated secretory phenotype (SASP)[10]. These data suggest the involvement of the ZsGreen cells and their pharmacological response in local inflammation and microglial activation in the Aβ plaque environment. Although a recent study suggested that astrocytes can acquire a senescence-like phenotype in patients with AD and in a tau-proteopathy animal model[11,31], we did not observe co-localization of astrocytes with cell senescence markers in Aβ plaques (see Supplementary Figs. 6b, 7b, 8a, and 9), and senolytic treatment did not reduce the numbers of plaque-associated astrocytes (Fig. 4c). In addition, there were no clear effects of D + Q treatment on the morphologies of Aβ plaque-associated astrocytes in our model (see Supplementary Figs. 17b and 19).

In peripheral organs, partial elimination of senescent cells (~30%) is sufficient to restore tissue homeostasis and function in disease models and during aging[7,29,30]. We next determined whether longterm intermittent senolytic treatment could ameliorate Aβ plaque pathology and/or improve cognition in APP/PS1 mice. Beginning at 3.5 months of age, female APP/PS1 AD mice were treated with either D + Q or vehicle once weekly for 11 weeks (Fig. 5a). Hippocampus-dependent spatial learning and memory were evaluated by testing the mice in the Y maze immediately before, and at the 6- and 11-week treatment time points, and mice were also tested in the water maze during treatment week 10. Mice were euthanized at 11 weeks and their brains processed for biochemical (one hemisphere) and histological (the other hemisphere) analyses. Aβ-plaque-associated SA-βGal activity in the hippocampus was greatly reduced in the AD mice that received the senolytic treatment compared with vehicle-treated AD mice (Fig. 5b). There was a significant reduction of Aβ-plaque-associated Olig2-immunoreactive cells in senolytic-treated AD mice, whereas there were no differences in numbers of Aβ-plaque-associated microglia and astrocytes (see Supplementary Fig. 21) in the D + Q-treated AD mice compared with vehicle-treated AD mice (Fig. 5b). Unlike the acute D + Q treatment, there was a highly significant reduction in Aβ plaque load in the hippocampus of D + Q-treated AD mice compared with vehicle-treated AD mice (Fig. 5b). We also found that senolytic treatment reduced levels of $A\beta_{40}$ and $A\beta_{42}$ in the hippocampus and entorhinal cortex of D + Q-treated AD mice compared with vehicle-treated AD mice (Fig. 5c), suggesting potential effects of the senolytic treatment on Aβ production and/or clearance. Consistent with A reduction in plaque-associated interleukin-6 levels in response to senolytic treatment (see Supplementary Fig. 20), the concentrations of the proinflammatory cytokines interleukin-1β (IL-1β) and tumor necrosis factor α (TNF-α) were significantly lower in the hippocampus of D + Q-treated AD mice compared with vehicle-treated AD mice (Fig. 5d). The IL-1β concentration in the entorhinal cortex was also significantly reduced in response to D + Q treatment. Interferon-γ concentrations were unaffected by D + Q treatment (Fig. 5d). Compared with vehicle-treated

APP/PS1 AD mice, APP/ PS1 AD mice treated with D + Q performed significantly better in the Y maze at both the 6- and the 11-week time points (Fig. 5f). In the water maze tests, D + Q treatment enhanced memory acquisition (more rapid learning of the location of the hidden platform) and memory retention in the probe trial (Fig. 5e).

Discussion

Our findings herein suggest that: (1) senescent cells that express OPC marker proteins are present in the Aβ plaque environment in the brains of patients with AD and the Aβ mouse AD model; (2) in Aβ plaques, OPCs become senescent with a proinflammatory phenotype, and in that state may be unable to differentiate into myelinating oligodendrocytes; (3) aggregating Aβ can act directly on OPCs to induce cellular senescence; (4) short-term (9 days) senolytic treatment removes p16-expressing OPCs from Aβ plaques in APP/PS1 mutant AD mice; (5) senolytic treatment reduces levels of Aβ-plaque-associated proinflammatory cytokine and microglial activation; (6) long-term (11 weeks), intermittent, senolytic treatment reduces neuroinflammation and Aβ plaque size, suggesting that senescent cells accelerate the development of Aβ pathology; and (7) senolytic treatment ameliorates hippocampus-dependent learning and memory deficits in the APP/PS1 AD mice, suggesting a role for cell senescence in the cascade of events by which Aβ accumulation causes cognitive impairment in AD (Fig. 5g).

Although AD is defined histopathologically by the accumulation of extracellular Aβ plaques and associated intraneuronal accumulation of hyperphosphorylated tau tangles, a rarer dementing disorder called frontotemporal dementia (FTD) is characterized by pTau tangles without Aβ plaques[32]. When the present manuscript was under review, two other laboratories provided evidence that astrocytes and microglia exhibit features of senescence in FTD tau mutant mice[11,12]. However, we did not detect astrocytes or microglia with senescent phenotypes in Aβ plaque microenvironments in the brains of APP/PS1 mice and human patients with AD. The FTD mouse studies employed SA-βGal staining as a marker of senescent cells in brain tissue sections. Although SA-βGal is widely used as a marker of senescence, some non-dividing cells, including neurons in the brains of young and aged wild-type mice, also exhibit relatively robust SA-βGal staining[21], emphasizing the necessity of using more specific markers of senescence. To this end, we employed the *p16* RNAscope-ISH technique and a novel ZsGreen/APPPS1 AD p16 reporter mouse line, along with a panel of senescence antibodies (p16 and p21) and glial antibody markers (OPCs, astrocytes, microglia, and oligodendrocytes). The results from the studies of the tau mice[11,12] and our analyses of APP/PS1 mice with Aβ plaques provide complementary insight into the responses of different types of glial cells to Aβ and tau pathologies. We observed an OPC senescence response to extracellular Aβ, and the other laboratories found astrocyte and microglial senescent responses to intracellular pTau pathology. Using a genetic approach[11] or FDA-approved D + Q senolytic drugs[12], the three studies demonstrate that the clearance of senescent cells is beneficial for ameliorating AD-related pathological phenotypes. It will therefore be of interest to elucidate mechanisms by which Aβ and pTau pathologies differentially affect OPCs, astrocytes, microglia, and oligodendrocytes in future studies. Nevertheless, the emerging findings therefore suggest that senescent cells contribute to the dysfunction and degeneration of neurons in AD and FTD.

Cellular senescence has been most extensively studied in peripheral tissues where cell turnover (proliferation, differentiation, and cell death) is robust. In such tissues, senescent cells accumulate during normal aging, and their SASP is believed to contribute to age-related tissue inflammation[33]. In contrast to proliferative tissues, the major cell populations in the brain are either postmitotic (neurons) or quiescent (astrocytes, oligodendrocytes, and microglia). Although there are neuronal stem cells in the dentate gyrus of the hippocampus and the subventricular zone, OPCs are the major proliferative cell in most brain regions[32]. In response to ischemic and traumatic brain injuries, OPCs migrate into the damaged tissue where they can differentiate into oligodendrocytes and remyelinate damaged axons[34]. In multiple sclerosis, OPCs can remyelinate axons in the early phase of the disease, but ultimately fail as the disease progresses[35–37]. It will therefore be of interest to determine whether OPC senescence contributes to neuroinflammation in multiple sclerosis. Our data suggest that OPCs undergo senescence in the Aβ plaque environment, where they may contribute to local inflammation and associated damage to neurons. Cellular senescence many also play a role in other neurodegenerative disorders, as suggested by a recent study that provides evidence that astrocytes undergo senescence in an animal model of Parkinson's disease[38].

We found that when cultured OPCs are exposed to aggregating $A\beta_{1–42}$ many of the cells undergo senescence, demonstrating that a high concentration of aggregating Aβ is sufficient to trigger cell senescence. In the brains of APP/PS1 mutant AD mice, senescent cells that express OPC markers (Olig2 and NG2) are present in the Aβ plaque environment, but not in regions devoid of Aβ, consistent with Aβ-inducing cell senescence. Our double-labeling immuno-histochemical analyses and analyses of p16 reporter mice suggest that the plaque-associated senescent cells are not microglia or astrocytes. We found that D + Q senolytic treatment kills senescent OPCs in culture, and removes senescent cells from the Aβ plaque environment in AD mice. The senolytic treatment resulted in a reduction in levels of proinflammatory cytokines which may be due, in part, to removal of OPCs with an SASP. However, direct anti-inflammatory effects of dasatinib and/or quercetin on microglia and astrocytes are also possible. In this regard, it will be of interest to cross AD mouse models with the recently reported transgenic mouse line in which p16-expressing cells can be selectively eliminated[8,9] to further elucidate roles for cell senescence in AD pathogenesis.

Using two different tests of hippocampus-dependent learning and memory, we found that long-term intermittent senolytic treatment improved cognition in APP/PS1 AD mice. This beneficial effect of senolytic therapy on brain function was associated with reduced Aβ plaque load in the hippocampus and reduced neuroinflammation. Both Aβ and inflammatory cytokines can impair synaptic plasticity[1,38–40], suggesting that the beneficial effects of senolytic treatment on cognition may result from suppression of inflammation and Aβ neurotoxicity. Whether the effect of D + Q on cognition results solely from removal of senescent cells or also involves actions of dasatinib or quercetin on neurons remains to be determined. Nevertheless, our findings pave the way for future preclinical and clinical studies that will test the hypothesis that senolytic therapies can suppress neuropathology and preserve brain function in AD and other age-related neurodegenerative disorders.

Online content

Any methods, additional references, Nature Research reporting summaries, source data, statements of data availability and associated accession codes are available at https://doi.org/10.1038/s41593-019-0372-9.

Methods

Transgenic mice, drug treatments, and human brain tissue.

Male APP/PS1 transgenic mice (B6.Cg-Tg(APPswe,PSENldE9)85Dbo; stock no. 34832), and age-and gender-matched wild-type controls, were obtained from the Jackson Laboratories. For generating a senescence reporter mouse line, the ZsGreen reporter gene driven by the pl6 promoter was made as described previously[7] except for a replacement of ATTAC by ZsGreen. In brief, a 2,617-base-pair segment of the murine pl6 promoter was amplified by PCR from the C57B6 genomic DNA using Platinum Pfx DNA Polymerase (Invitrogen) to replace a P2 promoter in a P2-ATTAC transgenic construct (a gift from P. Sherer), followed by subcloning the ZsGreen cDNA (Addgene, catalog no. 18121) to replace the ATTAC segment in pBlueScriptll. The inserts of pl6 promoter and ZsGreen were validated by full-range DNA sequencing and restriction mapping. Two transgenic founders were obtained by pronuclear injection of the p16 promoter-ZsGreen construct into FVB oocytes. A PCR-based method was used to identify the ZsGreen transgene (primer sequences are available upon request). ZsGreen females were mated with APP/PS1 males. Littermates with APP/PS1/ZsGreen were identified by PCR- based genotyping and used for pharmacological analysis at 5 months of age. The breeding colony was established in the National Institute on Aging Intramural Research Program vivarium. Mice were anesthetized with isofiurane and sequentially perfused transcardially with phosphate-buffered saline (PBS) and 4% paraformaldehyde in PBS. The fixed and sucrose-cryoprotected brain tissue was cut horizontally with a sliding microtome (Microm, HM440E) into 40-μm sections. All procedures were approved by the Animal Care and Use Committee of the National Institute on Aging Intramural Research Program.

Sixteen 3.5-month-old female APP/PS1 transgenic mice were randomly assigned to treatments by oral gavage with dasatinib and quercetin (Selleckchem) or vehicle once weekly for 11 weeks. Ten mixed gender, 8-month-old APP/PS1 mice, and eight 5-month-old APP/PS1/ZsGreen mice were randomly assigned to acute D + Q treatment with one dose daily for 4 days in the first week and 5 days in the second week. Dasatinib and quercetin were first dissolved in polyethylene glycol (PEG, Sigma-Aldrich) by sonication for 5 min, at a final concentration of 12 mg kg^{-1} of dasatinib and 50 mg kg^{-1} of quercetin in 20% PEG with 0.9% saline for treatment weeks 4–11. During the first 3 weeks the mice were treated with the same dose of D + Q in 30% PEG in distilled water, and this vehicle caused sickness behaviors in two of the mice. To test the blood-brain barrier permeabilities of D + Q, two APP/PS1 mice were subjected to D + Q oral administration and 2 h later the mice were perfused with 60 ml of cold PBS, and the hippocampus, cerebellum, and blood plasma were collected for measuring dasatinib levels by gas chromatography-mass spectrometry analysis using a Turbo Ion Spray module Sciex API 3000 triple-stage, quadrupole tandem mass spectrometer (ES/MS/MS; Sciex Inc.). We found that quercetin underwent considerable

metabolism within 2h of oral gavage (data not shown), similar to what has previously been reported[41].

Paraffin-embedded blocks of human postmortem tissue containing the inferior parietal lobule from people with AD, MCI, and NDC were acquired from the University of Kentucky Alzheimer's Disease Research Center, and were from well-characterized subjects with cognitive test results, Aβ plaque load, and Braak staging (see Supplementary Table 1).

Antibodies and reagents.

Antibodies were used that recognized $A\beta_{1–42}$ (rabbit polyclonal; Cell Signaling; catalog no. 2454) at dilutions of 1:300 to 1:1,000, $A\beta_{1–16}$ (Covance; clone 6E10, mouse monoclonal) at 1:300 to 1:1,000, NG2 (mouse monoclonal and rabbit polyclonal; EMD Millipore; catalog no. AB5320 and AB5384) at 1:100, MBP (rat monoclonal; EMD Millipore; catalog no. MAB386) at 1:200, OHg2 (IBL Immuno-Biological Laboratories Co; catalog no. 18953) at 1:100, Ibal (Wako Life Science; catalog no. 019–19741) at 1:100, GFAP (mouse monoclonal; BD Pharmingen; catalog no. 556329) at 1:500, $p21^{CDKN1A}$ (Santa Cruz Biotechnology; catalog no. sc397) at 1:100, CNP (mouse monoclonal; Santa Cruz Biotechnology; catalog no. sc-166063) at 1:100, pl6 (mouse monoclonal; Abeam; catalog no. ab54210) at 1:100, LAMP1 (rat monoclonal clone 1D4B; Developmental Studies Hybridoma Bank, University of Iowa and Santa Cruz Biotechnology Inc.; sc-19992) at 1:10 to 1:200, interleukin-6 (Cell Signaling Technology; catalog no. 12912) at 1:100, cleaved caspase-3 (Asp^{175}) (Cell Signaling; catalog no. 9661) at 1:1,000. The dye FSB was purchased from EMD Millipore and used at a dilution of 1:1,000. References to prior studies using these antibodies are cited in the text and/or are available at the vendor's website.

Histochemistry and immunohistochemistry.

Staining for SA-βGal was performed on free-floating mouse brain sections in the SA-βGal staining solution at 37 °C for 20–24h. The sections were briefly rinsed in PBS and then fixed in 4% paraformaldehyde for 10 min before processing for immunofluorescence. For counterstaining Aβ plaques, FSB, a derivative of Congo red-like, was dissolved in dimethylsulfoxide as a 10 mM stock and stored at −20 °C. After immunofluorescence staining, the sections were immersed in 1 μM FBS in PBS for 20 min, and examined with confocal microscopy using excitation and emission wavelengths of 390 and 511 nm. For immunohistochemical examinations, sections were pretreated with 1%H_2O_2 in PBS for 15 min to quench endogenous peroxidase activity. After blocking non-specific antigenicity with a blocking buffer (5% house serum, 3% bovine serum albumin (BSA), and 0.2% Triton 100 in PBS) for 1 h at room temperature, sections were incubated with anti-Aβ antibody overnight at 4°C, then incubated with a biotinylated anti-rabbit immunoglobulin G (1:200 dilution, Vector Laboratories). The antibody complex was detected using the peroxidase ABC system with DAB as the substrate following the manufacturer's instructions (Vector Laboratories). The sections were examined and images were acquired using a Nikon bright-field microscope (Nikon, Ellipse E600) with ×5, ×20,and ×40 objectives. Human brain tissue sections were deparaffinized, rehydrated, incubated in boiling citrate buffer (10 mM citric acid, 0.05% Tween 20, pH 6.0) for 10 min in a microwave, and then incubated in 75% formic acid (Sigma) for 10 min before immunofluorescence staining.

Free-floating mouse brain sections were incubated with blocking buffer (3% BSA, 5% normal serum, and 0.2% Triton X-100 in PBS) for 1 h, and then incubated with combinations of primary antibodies in blocking buffer overnight at 4°C. After thorough washes in PBS, sections were incubated with 1:400 dilution of Alexa 488-, Alexa 568-, and Alexa 647-conjugated secondary antibodies appropriate for the species of the primary antibodies, followed by FSB or DAPI counterstains. The sections were examined and images acquired using Leica-LMD7000, and Zeiss LSM510 and Zeiss LSM 880 AiryScan confocal laser-scanning confocal microscopes. For quantitation of SA-βGal and Aβ plaque load in bright-field images, images of a total area covering 2.3 mm^2 were acquired using a Leica-LMD7000 microscope with a × 10 objective. For quantitation of Aβ load, Aβ-associated OHg2, and p21 fluorescent intensities in fluorescence, 0.22 mm^2 frames were acquired using a Zeiss LSM510 microscope with a ×40 objective. Analyses were performed using Zeiss software (see Life Sciences Reporting Summary).

In situ hybridization.

Adult mouse brains were flash frozen and subjected to horizontal 10-μm-thick sections using cryostat and mounted on SuperFrost plus slides (Fisher Scientific) and stored at −80 °C. Sections were fixed in 4% paraformaldehyde for 15–20 min at 4°C, dehydrated in 50%, 70%, and 100% ethanol, air-dried at room temperature for 5 min and preincubated in proteinase IV solution for 30 min at room temperature. Fluorescent RNAscope-ISH was performed using an RNAscope Fresh Frozen Multiplex Fluorescent kit according to the manufacture's protocol (Advanced Cell Diagnostics, catalog no. 320293). Two probes recognizing mRNAs that encode mouse-housekeeping proteins (*Polr2a* and *Ppib* mRNAs) were used as the positive controls, and a probe recognizing the bacterial *DapB* gene was used as a negative control. A Cdkn2a-Cl (catalog no. 411011-Cl) probe that recognizes 79% *of p16* mRNA was purchased from Advanced Cell Diagnostics USA. Fluorescent images were captured on a Zeiss LSM 880 AiryScan laser-scanning confocal microscope with ×63 objective. The Z-stack projections were created using FIJI (ImageJ) software and three-dimensional reconstructions were created using Imaris 7.5.2 software (Bitplane Scientific Software).

Immunoelectron microscopy.

The procedures for pre-embedding immunoelectron microscopy have been described previously[42]. In brief, two APP/PS1 mice and two wild-type control mice (7.5 months old) were perfused transcardially with 4% paraformaldehyde, 0.16% glutaraldehyde, and 15% picric acid in 0.1 M phosphate buffer, pH 7.3. Brains were left in the same fixative solution for 2h at 4°C. The fixative solution was replaced with 2% paraformaldehyde and left overnight at 4°C. After rinsing with PBS, brains were cut into coronal serial sections (50 μm thick) with a vibratome (Leica) and incubated in a cryoprotective solution (25% sucrose, 10% glycerol with 2 μM NaN_3 in PBS) overnight at 4°C. The sections were flash frozen in liquid nitrogen and stored at −80 °C.

For silver-enhanced immunogold labeling, the sections were rinsed with PBS, and incubated with 1% sodium borohydride in PBS for 30 min to inactivate free aldehyde groups. After rinsing in PBS, the sections were incubated with blocking solution (5% normal goat serum,

3% BSA, and 0.02% saponin in PBS) for 30 min and then with a mixture of rabbit-anti-OHg2 (1:100 dilution) and mouse anti-Aβ (1:300 dilution) in blocking buffer for 24 h at 4°C. The sections were then rinsed thoroughly in PBS and incubated with a mixture of biotinylated goat-anti-mouse IgG (Vector Laboratories) and 1.4-nm gold-conjugated anti-rabbit IgG (Nanoprobes Inc.). After rinsing in PBS and double-distilled water, sections were incubated in a silver enhancement solution in the dark for 7 min (HQ silver enhancement kit, Nanoprobes Inc.). Next, the sections were sequentially processed with a standard ABC HRP kit and DAB Peroxidase (HRP) Substrate Kit (Vector Laboratories). After washes with PBS, the sections were post-fixed in 0.5% osmium tetroxide at room temperature for 30 min, and then incubated in 1% uranyl acetate for 2h in the dark. Sections were dehydrated with ethanol and propylene oxide, and flat embedded in PELCO Eponate 12 Kit. DAB-labeled Aβ plaques were dissected from embedded sections and remounted on blank plastic blocks, and cut with an ultramicrotome UC7 (Leica Microsystems Inc.) into thin (~ 70-nm) sections, collected on formvar-coated grids, counterstained with Reynolds lead citrate, and examined and photographed using a Tecnai G2 12 transmission electron microscope (FEI Company) equipped with a digital micrograph 3.4 camera (Gatan Inc.).

LCM and RT-qPCR analysis.

Three 9-month-old APP/PS1 mice and three agematched wild-type mice were employed for LCM analysis using a Zeiss PALM laser capture microdissection microscope. Flash-frozen brain tissue samples were cut into 10-μm sections using a cryostat microtome (Leica, CM3050s). Amyloid plaques were visualized by a rapid Aβ immunocytochemistry method using ImmPRESS HRP Anti-Rabbit IgG (Peroxidase) Polymer Detection Kit and ImmPACT DAB Peroxidase (HRP) Substrate kit following the manufacturer's protocol (Vector Laboratories). The sections were then post-fixed in ice-cold methanol for 10 min at 4°C. A Zeiss AxioObserver PALM microbeam with RoboMover cap system was used for imaging, and dissection and capture of tissue samples as illustrated in Supplementary Fig. 9. RNAs were extracted from the microdissected tissue samples using ARCTURUS PicoPure RNA Isolation Kit (Thermo Fisher Scientific). Reverse transcription followed by conventional PCR or by real-time quantitative (qPCR) analyses were performed as described previously[43]. The primers used to amplify each transcript are listed in Supplementary Table 2.

Mouse ESC-derived OPC culture, treatments, and analyses.

The mouse ESC line GFP-OHg2 was obtained from the American Type Culture Collection and maintained as described[22]. In brief, mESCs were cultured on irradiated, mouse embryonic fibroblast, feeder layers (GlobalStem) using Dulbecco's minimum essential medium (DMEM; Gibco) supplemented with 20% fetal bovine serum (Gibco), 2 mM L-glutamine (Gibco), 1 mM sodium pyruvate (Gibco), 0.1 mM β-mercaptoethanol (Gibco), 0.1 mM non-essential amino acids (NEAA; Gibco), and 1,000 Uml^{-1} leukemia inhibitory factor (Millipore). To induce sphere formation of embryoid bodies and neural stem cells, mESC colonies were trypsinized into single cells. The suspension cultures were first maintained for 2–3 days in differentiation medium (α-MEM supplemented with 20% knockout serum replacement, 1 mM sodium pyruvate, 0.1 mM NEAA, and 0.1 mM β-mercaptoethanol; all from Gibco). Retinoic acid (0.5 μM; Sigma), and purmorphamine (1 μM; Cayman

Chemical) and N2 supplement (Gibco) were added sequentially in the differentiation medium every 2 days. On day 9, embryoid bodies (EBs) were disaggregated in TrypLE (Invitrogen) and plated on 0.002% poly(L-ornithine)/50 μgml^{-1} laminin (Sigma)-coated dishes in OPC medium that consisted of 25% conditioned neurobasal medium from cortical neuron cultures at 5–7 days in vitro (DIV), and 75% DMEM/F12 medium with N2, B27, purmorphamine (1 μM), platelet-derived growth factor-AA (10 ngml^{-1}; Invitrogen), and fibroblast growth factor-2 (20ngml^{-1}; Millipore).

Synthetic Aβ_{1-42} (Bachem) was oligomerized as described[44]. Briefly, lyophilized Aβ_{1-42} was solubilized in 1,1,1,3,3,3-hexafluoro-2-propanol (HIFP; Sigma) to obtain monomers to a concentration of 5mM. Aβ_{1-42} /HFIP aliquots were dried in low-protein-binding tubes using a Speedvac and the resulting peptide film was stored at −80 °C until use. To generate oligomeric Aβ, the peptide was dissolved in dimethylsulfoxide to a concentration of 5mM, sonicated, and incubated overnight at 4°C. The peptide suspension was diluted in OPC medium to achieve the desired final concentrations. After 7days, the treated OPCs were assayed for SA-βGal activity.

Differentiated OPCs were rinsed with PBS, and then exposed to 10 Gy of ionizing radiation, further incubated in B27/N2 OPC medium for 10 days, and then treated with senolytic compounds containing 5 μM quercetin in combination with varying doses of dasatinib (0–1 μM) for 3 days. The apoptotic responses after senolytic treatments were measured by TUNEL staining using an In Situ Cell Death Detection kit (Fluorescein; Roche Applied Science) following the manufacturer's instructions, and immunoblotting using cleaved caspase-3 and PARP antibodies (Cell Signaling Technology).

FACS.

For detecting SA-βGal activity and cell viability in parallel, N2a neuroblastoma cells were seeded into six-well plates in the medium containing two parts DMEM and one part OptiMEM I with MEM NEAA and 5% fetal clone III. Cells reaching 70% confluence were exposed to ionizing radiation (10 Gy); 5 days later, non-irradiated and irradiated cell controls were incubated with 5 μM quercetin in combination with varying doses of dasatinib. Twenty-four hours after treatment with D + Q, irradiated and control cells were incubated in the fresh medium containing 300 μM chloroquine for 30 min at 37 °C, and sequentially incubated with fresh medium containing 33 μM C_{12}FDG, a fluorescent β-galactosidase substrate from ImaGene Green C_{12}FDG lacZ Gene Expression Kit (Molecular Probe, catalog no. I-2904) for 1 h at 37 °C. The cells were harvested by trypsinization and washed twice with cold PBS, and the cell pellets were suspended in flow cytometry buffer (2.5%BSA, 0.01%NaN_3 and 1 mM ethylenediaminetetraacetic acid in PBS). SA-βGal$^+$ cells were quantified by FACS and analysis of cell viability was performed in parallel after staining cells with 1 μgml^{-1} propidium iodide in flow cytometry buffer for 10 min. Control N2a cells were used for gating negative populations, and N2a cells irradiated with 10 Gy and treated with vehicle or the high dose of D + Q were used for gating positive populations of C_{12}FDG and propidium iodide staining, respectively. Then, 10,000–20,000 cells were analyzed per sample.

Behavioral testing and brain sample preparation.

APP/PS1 mice were subjected to the Y-maze spontaneous alternation and Morris water maze tests to evaluate short-term spatial memory[45]. On the days of behavioral evaluation, home cages were placed in the testing room 30 min before testing to allow habituation. All behavioral observations were made between 18:00 and 21:00. All equipment was cleaned between each trial. Short-term working memory was assessed in the Y-maze spontaneous alternation test using an opaque Perspex Y maze (38 cm long and 7.5 cm wide with 12 cm high walls). Each animal was placed in turn in arm A of the Y maze and allowed to explore for 5 min, and the arm entries and walking distance were recorded. Spontaneous alternation was defined as a successive entry into three different arms, on overlapping triplet sets. The percentage number of alternations was calculated as the number of actual alternations divided by the maximum number of alternations (the total number of arm entries minus 2). All experimental data were analyzed using the ANY-maze video tracking system (Stoelting Co.). Morris water maze spatial reference memory was assessed using a 1.2-m diameter, circular, white, opaque plastic tank that contained water maintained at a temperature of 22 ± 1 °C and made opaque using water-soluble non-toxic white paint. Briefly, for the acquisition of the 18-cm square hidden platform, the learning test was conducted for 5 days within 60 s of each trial and 4 times per day. After 24 h from the last acquisition test, a probe trial test was conducted without a hidden platform for 60 s to evaluate their memory retention. The mice performance (number of passing and distance in removed platform area) was determined using the ANY-maze video tracking system (Stoelting Co.).

Twenty-four hours after the last behavioral testing day, the mouse brains were dissected under deep anesthesia, and rinsed in cold PBS. One brain hemisphere was immediately fixed in 4% paraformaldehyde for 48 h at 4°C for SA-βGal and Aβ immunohistochemical analysis. The hippocampi, entorhinal cortex, and cerebellar regions in the other hemisphere were dissected in cold PBS and lysed in radioimmunoprecipitation assay buffer containing proteinase inhibitors. The soluble facture of lysates was collected for Aβ immunoassay with V-PLEX Aβ Peptide Panel (4G8) Kit (catalog no. K1519E) and cytokine immunoassay with Custom Mouse Cytokine kit (catalog no. K152A0H) according to the manufacturer's instructions (Meso Scale Diagnostics).

Statistical analyses.

All values are the mean and s.e.m. of the specific nature and number of replicates noted in the figure legends. The two-tailed Student's *t*-test was used for analysis of data from experiments that involved only two conditions (control and experimental treatment). One-way ANOVA with Dunnett's post-hoc test was performed for experiments that involved more than two conditions. No statistical methods were used to predetermine sample sizes; however, our sample sizes are similar to those reported in previous publications[46,47]. Data distribution was assumed to be normal, but this was not formally tested. For experiments with senolytic treatment, female APP/PS1 transgenic mice ($n = 16$) were randomly assigned to either D + Q treatment or vehicle control groups. Two mice in the vehicle control group were excluded because they exhibited sickness behaviors, apparently as a result of the oral gavage procedure. Laser capture RNA data collection and behavioral testing were performed in a blinded manner. All other data analyses were not performed blind to the conditions of

the experiments. For data shown as box-and-whisker plots in the figures and the supplementary figures, the box extends from the 25th to the 75th percentiles with the median shown as a line in the middle, and whiskers indicate the smallest and largest values. Analyses were performed using commercially available software (see Life Sciences Reporting Summary).

Reporting Summary.

Further information on research design is available in the Nature Research Reporting Summary linked to this article.

Supplementary Material

Refer to Web version on PubMed Central for supplementary material.

Acknowledgements

We thank N. Sah, J. Tian, and R. Munk for technical support. We thank D. Baker at the Mayo Clinic for his valuable advice about the use of senolytic agents in vivo. This research was supported by the Intramural Research Programs of the National Institute on Aging (NIA) and the National Institute on Drug Abuse, and by an NIA grant supporting the University of Kentucky Alzheimer's Disease Research Center (no. P30-AG0–28383).

References

1. Wyss-Coray T Inflammation in Alzheimer disease: driving force, bystander or beneficial response? Nat. Med 12, 1005–1015 (2006). [PubMed: 16960575]
2. Nixon RA The role of autophagy in neurodegenerative disease. Nat. Med 19, 983–997 (2013). [PubMed: 23921753]
3. Scheltens P et al. Alzheimer's disease. Lancet 388, 505–517 (2016). [PubMed: 26921134]
4. Malm TM, Jay TR & Landreth GE The evolving biology of microglia in Alzheimer's disease. Neurotherapeutics 12, 81–93 (2015). [PubMed: 25404051]
5. Muñoz-Espín D & Serrano M Cellular senescence: from physiology to pathology. Nat. Rev. Mol. Cell Biol 15, 482–496 (2014). [PubMed: 24954210]
6. Rodier F & Campisi J Four faces of cellular senescence. J. Cell Biol. 192, 547–556 (2011). [PubMed: 21321098]
7. Baker DJ et al. Clearance of p16Ink4a-positive senescent cells delays ageing-associated disorders. Nature 479, 232–236 (2011). [PubMed: 22048312]
8. Baker DJ et al. Naturally occurringp16(Ink4a)-positive cells shorten healthy lifespan. Nature 530, 184–189 (2016). [PubMed: 26840489]
9. Childs BG et al. Senescent intimal foam cells are deleterious at all stages of atherosclerosis. Science 354, 472–477 (2016). [PubMed: 27789842]
10. Xu M et al. Senolytics improve physical function and increase lifespan in old age. Nawt. Med 24, 1246–1256 (2018).
11. Bussian TJ et al. Clearance of senescent glial cells prevents tau-dependent pathology and cognitive decline. Nature 562, 578–582 (2018). [PubMed: 30232451]
12. Musi N et al. Tau protein aggregation is associated with cellular senescence in the brain. Aging Cell 17, e12840 (2018). [PubMed: 30126037]
13. Geha S et al. NG2+/Olig2+ cells are the major cycle-related cell population of the adult human normal brain. Brain Pathol. 20, 399–411 (2010). [PubMed: 19486010]
14. Kang SH, Fukaya M, Yang JK, Rothstein JD & Bergles DE NG2+CNS glial progenitors remain committed to the oligodendrocyte lineage in postnatal life and following neurodegeneration. Neuron 68, 668–681 (2010). [PubMed: 21092857]

15. Clemente D, Ortega MC, Melero-Jerez C & de Castro F The effect of glia-glia interactions on oligodendrocyte precursor cell biology during development and in demyelinating diseases. Front. Cell. Neurosci 7, 268 (2013). [PubMed: 24391545]
16. Jennings AR & Carroll WM Oligodendrocyte lineage cells in chronic demyelination of multiple sclerosis optic nerve. Brain Pathol. 25, 517–530 (2015). [PubMed: 25175564]
17. Dimri GP et al. A biomarker that identifies senescent human cells in culture and in aging skin in vivo. Proc. Natl Acad. Sci. USA 92, 9363–9367 (1995). [PubMed: 7568133]
18. Kurz DJ, Decary S, Hong Y & Erusalimsky JD Senescence-associated (beta)-galactosidase reflects an increase in lysosomal mass during replicative ageing of human endothelial cells. J. Cell Sci. 113, 3613–3622 (2000). [PubMed: 11017877]
19. Debacq-Chainiaux F, Erusalimsky JD, Campisi J & Toussaint O Protocols to detect senescence-associated beta-galactosidase (SA-betagal) activity, a biomarker of senescent cells in culture and in vivo. Nat. Protoc 4, 1798–1806 (2009). [PubMed: 20010931]
20. Borchelt DR et al. Accelerated amyloid deposition in the brains of transgenic mice coexpressing mutant presenilin 1 and amyloid precursor proteins. Neuron 19, 939–945 (1997). [PubMed: 9354339]
21. Piechota M et al. Is senescence-associated β-galactosidase a marker of neuronal senescence? Oncotarget 7, 81099–81109 (2016). [PubMed: 27768595]
22. Zhan X et al. Myelin basic protein associates with AβPP, Aβ1–42, and amyloid plaques in cortex of Alzheimer's disease brain. J. Alzheimers Dis 44, 1213–1229 (2015). [PubMed: 25697841]
23. Jiang P et al. Generation and characterization of spiking and nonspiking oligodendroglial progenitor cells from embryonic stem cells. Stem Cells 31, 2620–2631 (2013). [PubMed: 23940003]
24. Meijer DH et al. Separated at birth? The functional and molecular divergence of OLIG1 and OLIG2. Nat Rev. Neurosci 13, 819–831 (2012). [PubMed: 23165259]
25. Condello C, Yuan P, Schain A & Grutzendler J Microglia constitute a barrier that prevents neurotoxic protofibrillar Aβ42 hotspots around plaques. Nat. Commun 6, 6176 (2015). [PubMed: 25630253]
26. Gowrishankar S et al. Massive accumulation of luminal protease-deficient axonal lysosomes at Alzheimer's disease amyloid plaques. Proc. Natl Acad. Sci. USA 112, E3699–E3708 (2015). [PubMed: 26124111]
27. Barrachina M, Maes T, Buesa C & Ferrer I Lysosome-associated membrane protein 1 (LAMP-1) in Alzheimer's disease. Neuropathol. Appl. Neurobiol 32, 505–516 (2006). [PubMed: 16972884]
28. Nixon RA et al. Extensive involvement of autophagy in Alzheimer disease: an immuno-electron microscopy study. J. Neuropathol. Exp. Neurol 64, 113–122 (2005). [PubMed: 15751225]
29. Zhu Y et al. The Achilles' heel of senescent cells: from transcriptome to senolytic drugs. Aging Cell 14, 644–658 (2015). [PubMed: 25754370]
30. Farr JN et al. Targeting cellular senescence prevents age-related bone loss in mice. Nat. Med 23, 1072–1079 (2017). [PubMed: 28825716]
31. Bhat R et al. Astrocyte senescence as a component of Alzheimer's disease. PLoS One 7, e45069 (2012). [PubMed: 22984612]
32. Rademakers R, Neumann M & Mackenzie IR Advances in understanding the molecular basis of frontotemporal dementia. Nat. Rev. Neurol 8, 423–434 (2012). [PubMed: 22732773]
33. LeBrasseur NK, Tchkonia T & Kirkland JL Cellular senescence and the biology of aging, disease, and frailty. Nestle Nutr. Inst. Workshop Ser 83, 11–18 (2015). [PubMed: 26485647]
34. Baker DJ & Petersen RC Cellular senescence in brain aging and neurodegenerative diseases: evidence and perspectives. J. Clin. Invest 128, 1208–1216 (2018). [PubMed: 29457783]
35. Neumann B & Kazanis I Oligodendrocyte progenitor cells: the ever mitotic cells of the CNS. Front. Biosci. (Schol. Ed.) 8, 29–43 (2016). [PubMed: 26709894]
36. Zhang R, Chopp M & Zhang ZG Oligodendrogenesis after cerebral ischemia. Front Cell. Neurosci 7, 201 (2013). [PubMed: 24194700]
37. Antel JP et al. Immunology of oligodendrocyte precursor cells in vivo and in vitro.J. Neuroimmunol 10.1016/j.jneuroim.2018.03.006 (2018).

38. Chinta SJ et al. Cellular senescence is induced by the environmental neurotoxin paraquat and contributes to neuropathology linked to Parkinson's disease. Cell Rep. 22, 930–940 (2018). [PubMed: 29386135]

39. Mattson MP Pathways towards and away from Alzheimer's disease. Nature 430, 631–639 (2004). [PubMed: 15295589]

40. Salter MW & Stevens B Microglia emerge as central players in brain disease. Nat. Med 23, 1018–1027 (2017). [PubMed: 28886007]

41. Yang LL et al. Pharmacokinetic comparison between quercetin and quercetin 3-O-β-glucuronide in rats by UHPLC-MS/MS. Sci. Rep 6, 35460 (2016). [PubMed: 27775094]

42. Zhang S et al. Dopaminergic and glutamatergic microdomains in a subset of rodent mesoaccumbens axons. Nat. Neurosci 18, 386–392 (2015). [PubMed: 25664911]

43. Zhang P et al. Novel RNA- and FMRP-binding protein TRF2-S regulates axonal mRNA transport and presynaptic plasticity. Nat. Commun 6, 8888 (2015). [PubMed: 26586091]

44. Stine WB Jr., Dahlgren KN, Krafft GA & LaDu MJ In vitro characterization of conditions for amyloid-beta peptide oligomerization and fibrillogenesis./. Biol. Chem 278, 11612–11622 (2003).

45. Faucher P, Mons N, Micheau J, Louis C & Beracochea DJ Hippocampal injections of oligomeric amyloid β-peptide (1–42) induce selective working memory deficits and long-lasting alterations of ERK signaling pathway. Front. Aging Neurosci 7, 245 (2016). [PubMed: 26793098]

46. Kashiwaya Y et al. A ketone ester diet exhibits anxiolytic and cognition- sparing properties, and lessens amyloid and tau pathologies in a mouse model of Alzheimer's disease. Neurobiol. Aging 34, 1530–1539 (2013). [PubMed: 23276384]

47. Sykora P et al. DNA polymerase β deficiency leads to neurodegeneration and exacerbates Alzheimer disease phenotypes. Nucleic Acids Res. 43, 943–959 (2015). [PubMed: 25552414]

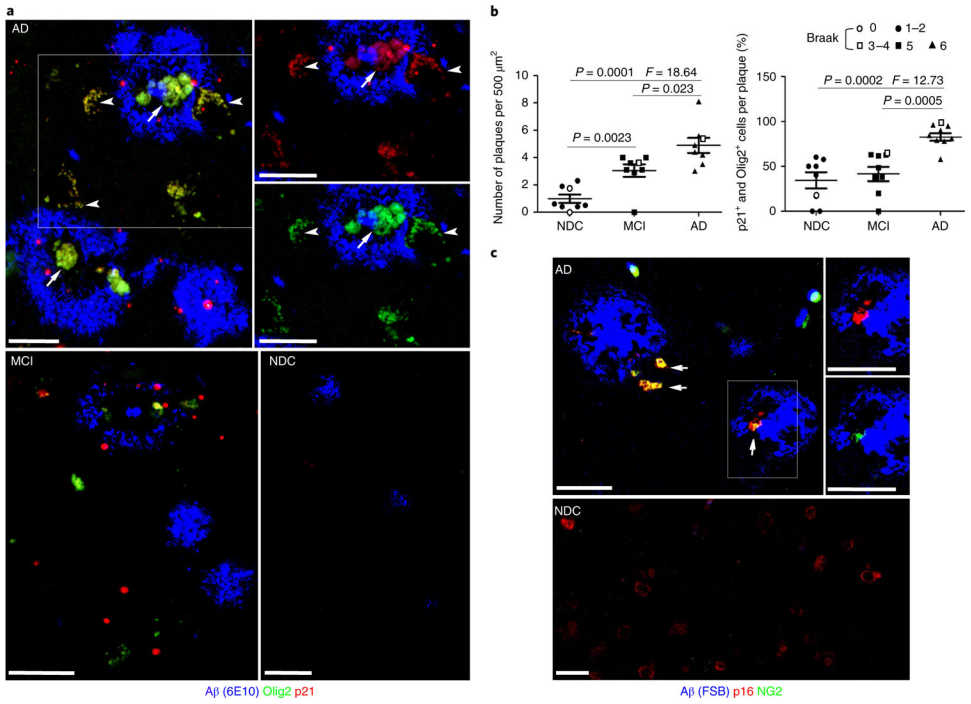

Fig. 1|. OPCs exhibiting a senescence phenotype are associated with Aβ plaques in brains of patients with AD.

a, Confocal images showing Aβ (blue), Olig2 (green), and p21 (red) immunoreactivities in sections of inferior parietal cortex from a patient with AD, a patient with MCI, and an NDC subject. Arrows point to Aβ-associated cells that exhibit both Olig2 and p21 immunoreactivities (yellow). Arrowheads point to processes of OPCs associated with an Aβ plaque. The two panels at the upper right are higher magnifications of the plaque in the boxed area, **b,** Average numbers of Aβ plaques per 500 μm^2 (left) and percentages of Aβ plaques harboring one or more p21 and Olig2 double-positive cells (right) (mean ± s.e.m.; *n = 8* AD, 8 MCI, and 8 NDC subjects; 20 images analyzed in sections from MCI and AD brains and 10 images analyzed in sections from NDC brains). The statistical analysis was performed using one-way ANOVA followed by Dunnett's post hoc tests. The symbols in the key shown above the graphs denote the Braak stage score for each subject, **c,** Confocal images showing FSB staining of labeled fibrillary Aβ (blue), p16 (red), and NG2 (green) immunoreactivities, in sections of inferior parietal cortex from a patient with AD and an NDC subject (these images are representative of images from brain sections from three patients with AD and three NDC subjects). Arrows point to Aβ-associated cells that exhibit both p16 (red) and NG2 (green) immunoreactivities. Scale bars, 20 μm.

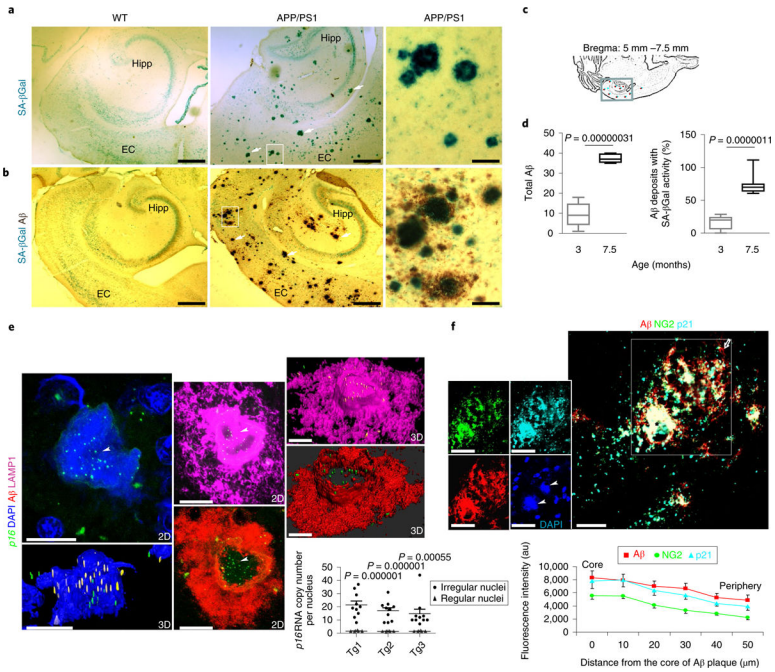

Fig. 2 |. Association of cellular senescence and OPC markers with Aβ plaques in the brains of APP/PS1 double-mutant transgenic mice.

a,b, SA-βGal staining alone **(a)** or in combination with Aβ immunohistochemical staining **(b)** in horizontal brain sections from 7.5-month-old APP/PS1 transgenic mice and wild-type (WT) littermate controls. Arrows point to SA-βGal foci and their associations with Aβ plaques. The rightmost panels show high magnification of the areas demarcated by the boxes in the middle panels. Hipp, hippocampus; EC, entorhinal cortex. Scale bars: left and middle panels, 100 μm; right panels, 40 μm. Images are representative of those observed in brain sections from three WT mice and three APP/PS1 transgenic mice (three sections examined from each brain), **c,** The box in the schematic illustration demarcates the hippocampal formation, from which counts of Aβ plaques and Aβ plaques with SA-βGal foci were made in brain sections of APP/PS1 mutant transgenic mice, **d,** The graphs show the Aβ load and percentage of Aβ plaques with SA-βGal activity in 3-month-old and 7.5-month-old APP/PS1 mice. Analyses were performed on three mice of each age (three sections from each brain were analyzed); significance was determined using the two-tailed Student's *t*-test. **e,** Representative confocal images showing the intracellular accumulation of *p16* mRNAs within an Aβ plaque in the brain of an 8-month-old APP/PS1 mouse. Arrowheads point to numerous copies of *p16* mRNA (yellow and green puncta in two-dimensional (2D) and three-dimensional (3D) images representing *p16* RNAs) and their spatial relationships with Aβ (red) as well as the intracellular organelles, lysosomal-associated membrane protein 1 (LAMPI)-labeled lysosomes (pink), and 4,6-diamidino-2-phenylindole (DAPI)-labeled nuclei (blue); scale bar,15μm. Also see the 3D animations in Supplementary Videos 1, 2, and 3. The images are representative of 12–15 plaque-associated cells examined per brain ($n = 3$ mice). The graph shows a comparison of the *pl6* mRNA levels in Aβ-associated cells, and cells not associated with Aβ. Values are the mean and s.e.m. ($n = 3$ mice per group); significance is determined using the two-tailed Student's *t*-test. Tgl, Tg2, and Tg3 denote three different APP/PS1 mutant transgenic mice, **f,** Confocal images showing Aβ deposit-

associated cells exhibiting the co-localization of Aβ immunoreactivity (red) with the OPC (green) and the senescence marker p21 (cyan blue) in a brain section from a 7.5-month-old APP mouse. The leftmost inserts are unmerged images in the boxed area. Arrowheads point to DAPI-labeled irregular nuclei in the plaque. The asterisk and open arrow mark the core and periphery of the Aβ plaque, respectively. Scale bar, 20 μm. The images are representative of those observed in brain sections from 3 different mice (25 plaques examined from each brain). The graph shows the relative fluorescence intensities of the indicated protein markers from the core to the peripheral edge of the plaque (values are the mean and s.e.m. of measurements made on 25 plaques).

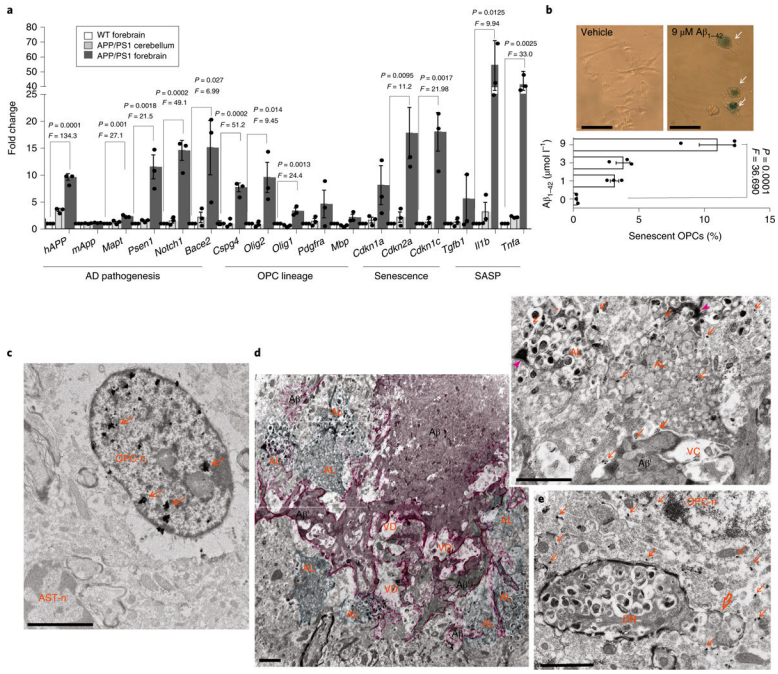

Fig. 3 |. Molecular and ultrastructural features of Aβ-associated OPC senescence.

a, Relative levels of the indicated mRNAs in laser-captured tissue samples from the forebrain of wild-type (WT, white bars) mice, and plaque-bearing forebrain (gray bars) and plaque-free cerebellar tissues (light gray bars) of APP/PS1 mice. Levels of the mRNAs were normalized to the levels of *Actb* mRNA in the same sample and values were expressed as fold change (mean and s.e.m.; $n = 3$ mice per group). The statistical analysis was performed with one-way ANOVA followed by Dunnett's post hoc tests, **b,** Exposure to $A\beta_{1–42}$ triggers cellular senescence in mouse embryonic stem cell-derived OPCs. On exposure to pre-aggregating $A\beta_{1–42}$ or vehicle for 7 days, OPC cultures were assayed for SA-βGal activity. Arrows point to enlarged senescent OPCs. The graph shows the percentage of SA-βGal$^+$ cells (values are the mean and s.e.m. of determinations made on 150–200 cells in 3 independent experiments). The statistical analysis was performed with one-way ANOVA followed by Dunnett's post hoc tests. Scale bar, 20 μm. **c–e,** Forebrain tissues from 7.5-month-old APP/PS1 mutant mice were processed for double-labeled, preembedding, immunoelectron microscopy using antibodies against Olig2 (immunogold particles) and Aβ (3,3'-diaminobenzidine (DAB) reaction product). Scale bars, 2μm. **c,** Electron micrograph showing Olig2 immunolabeling exclusively located in the nucleus of an OPC (OPC-n) from a region of cerebral cortex devoid of Aβ. Arrows point to Olig2$^+$silver-enhanced gold particles. Note that there is no Olig2 immunoreactivity in the nucleus of an adjacent astrocyte (AST-n). **d,** Electron micrographs showing the core (Aβ) and the periphery branches (Aβ') of an amyloid plaque (pink shading). Cells located in the Aβ plaque environment are filled with autolysosomes (green shading). The upper right insert is a higher magnification of boxed area showing Olig2$^+$immunogold particles in the cytoplasm and autolysosomes (arrows). Arrowheads point to an Aβ deposit directly contacting a cell filled with autolysosomes; AL, autolysosomes; VD, region of vacuolar degeneration, **e,** Electron micrograph showing a lightly myelinated (open arrow) dystrophic neurite filled with

autolysosomes. An Olig2^{+} OPC is closely associated with the dystrophic neurite. OPC-n, OPC nucleus. Images are representative of 7 brain regions devoid of Aβ and 24 brain regions with plaques examined.

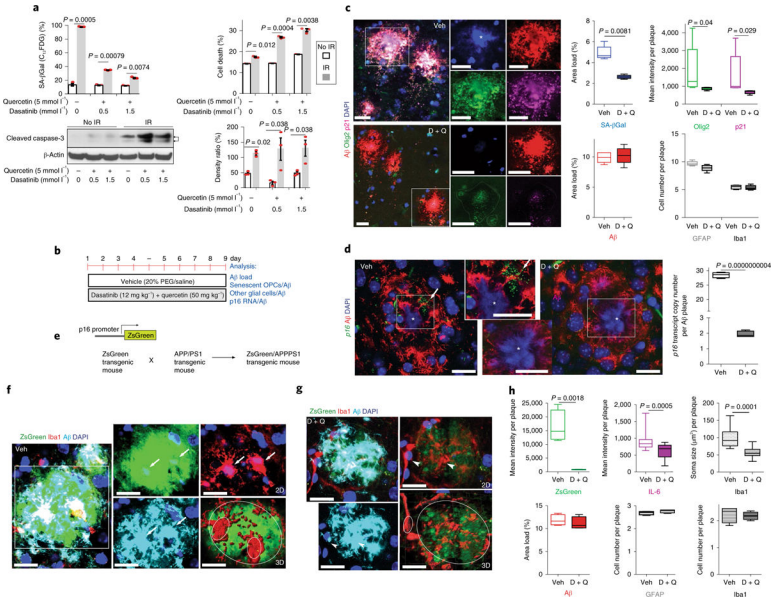

Fig. 4 |. Senolytic treatment selectively kills p16- and p21-expressing OPCs from the Aβ plaque environment in AD mice.

a, N2a cells were first exposed to ionizing radiation (IR; 10 Gy) to induce replicative senescence; 5 days later cells were treated with the indicated concentrations of D + Q for 24 h before FACS and immunoblot analysis. Top: graphs showing quantification of SA-βGal activity and cell viability by FACS. Bottom: cleaved caspase-3 immunoblot and graph showing results of densitometric analysis (samples from $n = 3$ mice; significance determined using the two-tailed Student's *t*-test). **b,** Experimental design for 9-day administration of D + Q once daily in 7.5-month-old APP/PS1 mice, **c,** The images show Aβ, Olig2, and p21 immunoreactivities in brain sections from APP/PS1 mice treated with vehicle (Veh, upper panels) or D + Q (lower panels) for 9 days. The graphs show the results of quantifications of Aβ load and plaque-associated SA-βGal, Olig2, p21, Ibal, and GFAP immunoreactivities. Values are the mean and s.e.m. of determinations made on 5 mice per group (12–15 plaques analyzed per mouse), **d,** Confocal images and graphs showing the level of *p16* RNAs in Aβ plaques from the brains of APP/PS1 mice that underwent short-term treatment with vehicle or D + Q. The arrow points to a cluster of *p16* mRNA puncta accumulated in the cytoplasm next to a nucleus (*) within the Aβ environment in the vehicle-treated mouse. Values are the mean and s.e.m. of determinations made on 3 mice per group (12–15 plaques analyzed per mouse), **e,** Breeding scheme for generating APP/PS1 double-mutant senescence reporter mice. **f,g,** Images showing Aβ (cyan) and Ibal (red) immunoreactivities and ZsGreen fluorescence (p16 reporter) in plaques of APP/PS1 AD mice that underwent 9-day treatment with either vehicle **(f)** or D + Q **(g).** Arrows **(f),** arrowheads **(g),** and small circles in three-dimensional images indicate activated microglia and deactivated microglia, respectively. Scale bar,20μm. **h,** Graphs show levels of ZsGreen fluorescence intensity per plaque, Aβ plaque load, GFAP-immunoreactive cells per plaque, interleukin-6 (IL-6) level/plaque, the soma size, and cell number of Iba1^{+}microglia/plaque in vehicle- and D + Q-treated mice. Values are the mean and s.e.m. of determinations made on 3 mice per group (12–15 plaques analyzed per mouse).

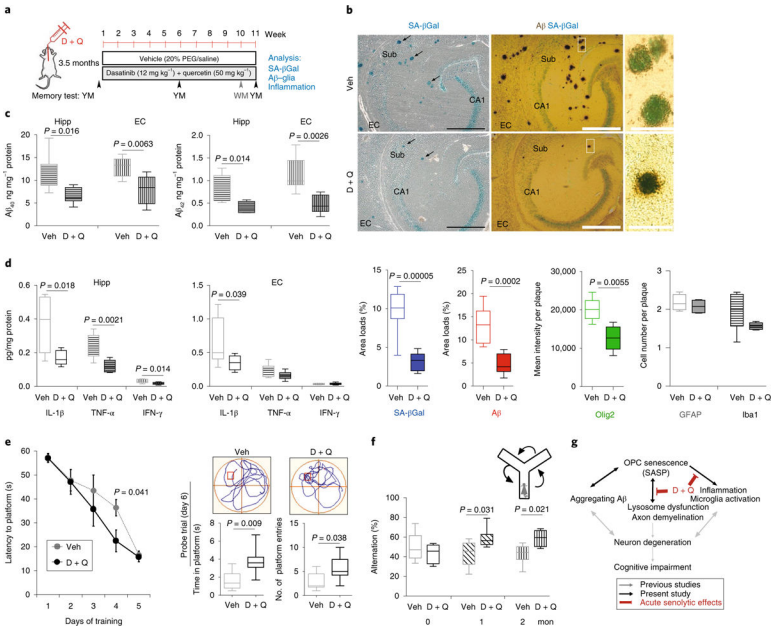

Fig. 5 |. Long-term senolytic treatment prevents Aβ accumulation and hippocampus-dependent cognitive impairment in APP/PS1 AD mice.

a, Experimental design for 11-week intermittent administration (once per week beginning at 3.5 months of age) of D + Q and vehicle control in female APP/PS1 mice. YM, Y maze; WM, water maze. PEG, polyethylene glycol, **b,** Images of hippocampus from the brain sections in the vehicle (Veh) control group (upper) and in the D + Q group (lower) showing SA-βGal staining (blue) alone (left) and in combination with Aβ immunohistochemical staining (brown) (middle). Arrows point to Aβ plaque-associated SA-βGal staining. Right: high-magnification views of the boxed areas shown in the middle panels. Scale bars: left and middle,100 μm; right, 40 μm. The graphs show the results of quantitative analysis of SA-βGal staining, Aβ load, and plaque-associated Olig2-, Ibal-, and GFAP-immunoreactive cells in the hippocampus in vehicle (open bars) and D + Q (solid bars) groups. All values are the mean and s.e.m. of measurements made on five sections per mouse from vehicle (six mice) and D + Q (eight mice) groups. Sub, subiculum. **c,d,** Graphs showing concentrations of $A\beta_{40}$ and $A\beta_{42}$ **(c)** and cytokines **(d)** in lysates of hippocampus (Hipp) and entorhinal cortex (EC) from mice in the D + Q *(n* = 8) and vehicle *(n* = 6) groups. Values are the mean and s.e.m. IFN-γ, interferon-γ. e, Water maze test. Goal latencies during the 5-day acquisition training trials (left), and a probe trial performed 24 h after the final day of training (right). On training day 4 the D + Q group *(n* = 8 mice) took significantly less time to reach the hidden platform compared with mice in the vehicle control group *(n* = 6 mice). In the probe trial the D + Q group spent significantly more time in the platform area and had significantly more platform-site entries, compared with the vehicle control group. The swimming paths in the probe trial of representative mice in the vehicle and D + Q groups are shown above the graphs (the red square marks the location where the platform had been during the goal acquisition trials). Significance was determined using the two-tailed Student's *t*-test. f, Top: schematic of the Y-maze working memory task. Bottom: percentage of spontaneous alternations were measured at baseline and during experimental weeks 6 and 11 for the D + Q group *(n* = 8) and the vehicle group *(n* = 6). All values are the mean and

s.e.m. (ANOVA with Dunnett's post hoc tests), **g,** A working model for the involvement of OPC senescence in the pathogenesis of AD. OPCs are recruited into developing Aβ plaques where the aggregating Aβ induces OPC senescence. The SASP of the OPCs may trigger or enhance the local activation of microglia and production of proinflammatory cytokines. A positive feedback among aggregating Aβ, senescent OPCs, and inflammation may cause demyelination and neuronal dysfunction and degeneration, resulting in cognitive impairment. D + Q senolytic treatment rapidly eliminates senescent OPCs and reduces neuroinflammation and, with continued intermittent treatment, reduces Aβ accumulation and ameliorates cognitive deficits. Black and gray arrows indicate the processes supported by data in the present study and previous studies[2,5], respectively. Acute senolytic effects are shown in red.

Table 1|

Glial-type identity of ZsGreen senescent cells in Aβ plaques.

Cell type	Antibody marker	No. of Aβ plaques	No. of ZsGreen$^+$ cells	No. of ZsGreen$^-$ cells
OPC	Olig2	34	34[a]	0
Oligodendrocyte	CNP	32	2	30
Astrocyte	GFAP	15	0	32
Microglia	Ibal	19	0	42

[a]A flattened Olig2$^+$SA-Galβ$^+$ ZsGreen cell profile was counted as a single cell. CNP, 2',3'-cyclic- nucleotide 3'-phosphodiesterase.